

Quantifying Kinematic Substructure in the Milky Way's Stellar Halo

Xiang-Xiang Xue^{1,2}, Hans-Walter Rix², Brian Yanny³, Timothy C. Beers⁴, Eric F. Bell^{5,2}, Gang Zhao¹, James S. Bullock⁶, Kathryn V. Johnston⁷, Heather Morrison⁸, Constance Rockosi⁹, Sergey E. Koposov^{10,2,11}, Xi Kang^{12,2}, Chao Liu², Ali Luo¹, Young Sun Lee⁴, Benjamin. A. Weaver¹³

ABSTRACT

We present and analyze the positions, distances, and radial velocities for over 4000 blue horizontal-branch (BHB) stars in the Milky Way's halo, drawn from SDSS DR8. We search for position-velocity substructure in these data, which is expected from hierarchical galaxy formation models, where most of the halo stars are still-detectable tidal debris from disrupted satellite galaxies. Using a cumulative “close pair distribution” (CPD) as a statistic in the 4-dimensional space of sky position, distance, and velocity, we quantify the presence of position-velocity

¹Key Lab of Optical Astronomy, National Astronomical Observatories, CAS, 20A Datun Road, Chaoyang District, 100012, Beijing, China

²Max-Planck-Institute for Astronomy Königstuhl 17, D-69117, Heidelberg, Germany

³Fermi National Accelerator Laboratory, P.O. Box 500 Batavia, IL 60510-5011, USA

⁴Department of Physics and Astronomy and JINA: Joint Institute for Nuclear Astrophysics, Michigan State University, E. Lansing, MI 48824, USA

⁵Department of Astronomy, University of Michigan, 500 Church Street, Ann Arbor, Michigan, 48109, USA

⁶Center for Cosmology, Department of Physics and Astronomy, University of California, Irvine, CA 92697, USA

⁷Astronomy Department, Columbia University, New York, NY 10027, USA

⁸Department of Astronomy, Case Western Reserve University, Cleveland, OH 44106, USA

⁹Lick Observatory/University of California, Santa Cruz, CA 95060, USA

¹⁰Institute of Astronomy, Madingley Road, Cambridge CB3 0HA, UK

¹¹Sternberg Astronomical Institute, Universitetskiy pr. 13, 119992 Moscow, Russia

¹²Purple Mountain Observatory, CAS, 2 West Beijing Road, Nanjing, 210008, China

¹³Center for Cosmology and Particle Physics, New York University, New York, NY 10003, USA

substructure at high statistical significance among the BHB stars: pairs of BHB stars that are close in position on the sky tend to have more similar distances and radial velocities compared to a random sampling of these overall distributions. We make analogous mock-observations of 11 numerical halo formation simulations, in which the stellar halo is entirely composed of disrupted satellites debris, and find a level of substructure comparable to that seen in the actually observed BHB star sample. This result quantitatively confirms the hierarchical build-up of the stellar halo through a signature in phase (position-velocity) space. In detail, the structure present in the BHB stars is somewhat less prominent than that seen in most simulated halos, quite possibly because BHB stars represent an older sub-population. BHB stars located in the outer halo, beyond 10 kpc from the Galactic center, exhibit statistically stronger substructure signatures than at $r_{\text{gc}} < 10$ kpc.

Subject headings: Cosmology: stellar halo — galaxies: individual(Milky Way) — Galaxy: halo — Galaxy: substructure — stars: horizontal-branch — stars: kinematics

1. Introduction

The current hierarchical structure formation paradigm implies that the formation of our Milky Way entailed a sequence of dark matter driven accretion and merger events (Searle & Zinn 1978; White & Rees 1978; Blumenthal et al. 1984). This naturally results in the expectation that the stellar halo should be largely built up from stars of tidally disrupted satellite galaxies, resulting in substructure that may appear as stellar streams with different degrees of phase-mixing (e.g. Bullock et al. 2001; Bullock & Johnston 2005, hereafter BJ05; Cooper et al. 2010). Because stars are gravitationally collisionless systems, their phase-space (spatial and velocity) distributions encode and retain aspects of their origin. This implies that an analysis of substructure in the position-velocity distribution of stars in the halo is a direct test for hierarchical models of galaxy formation.

In the past decades, observational evidence of spatial substructure has indeed been found in the Milky Way, both near the Sun (Majewski et al. 1996; Helmi et al. 1999) and at larger distances (Ibata et al. 1994, 1995). The most prominent example is the discovery of the Sagittarius dwarf galaxy (Ibata et al. 1994, 1995; Yanny et al. 2000) and its trails of debris (Ibata et al. 2001; Majewski et al. 2003).

In nearby samples of stars, where the full 6D phase-space coordinates can be measured,

substructure in the stellar distribution is seen in velocity space, or even in the integrals of motion (Dehnen & Binney 1998; Helmi et al. 1999; Klement et al. 2008, 2009; Morrison et al. 2009; Smith et al. 2009). At distances from the Sun characteristic of the stellar halo, ~ 20 kpc, individual transverse velocities are all but impossible to measure from proper motions with current technology. The available observables are therefore the position in the sky, a distance estimate from photometric or spectroscopic luminosity determinations, and line-of-sight velocity: α, δ, d , and V_{los} . When averaged over large angular areas and broad distance ranges, the line-of-sight kinematics of the Milky Way halo stars at 10-50 kpc are well-described by a simple Gaussian with $\sigma_{los} \approx 111 \text{ km s}^{-1}$ (Xue et al. 2008, hereafter X08). However, because the stellar halo is collisionless, preserving phase-space density, substructure in position space necessarily implies substructure in velocity space. Recent work by Starkenburg et al. (2009) and De Propris et al. (2010) indicate that the Milky Way’s stellar halo indeed possesses detectable position-velocity substructure. Schlaufman et al. (2009) have shown that metal-poor halo stars within ~ 17.5 kpc from the Sun exhibit clear evidence for velocity clustering on very small spatial scales (which the authors refer to as Elements of Cold Halo Substructure, or ECHOS).

With the development of large-scale sky surveys, such as the Two Micron All Sky Survey (2MASS; Skrutskie et al. 2006), the Sloan Digital Sky Survey (SDSS; York et al. 2000; Stoughton et al. 2002; Abazajian et al. 2003, 2004, 2005, 2009; Adelman-McCarthy et al. 2006, 2007, 2008), and the follow-up SEGUE survey (Yanny et al. 2009b), we have an unprecedented opportunity to examine Milky Way halo streams in detail (Ivezić et al. 2000; Yanny et al. 2000; Newberg et al. 2002; Majewski et al. 2003; Yanny et al. 2003; Newberg et al. 2007; Yanny et al. 2009a). Halo star samples are now of sufficient size and quality that a direct statistical comparison with models, such as BJ05, has become possible.

A first quantitative comparison indicated that the observed level of *spatial* substructure (on all scales) is similar to that expected from those simulations, where the halo is composed entirely of disrupted satellites (Bell et al. 2008, hereafter B08). Imaging surveys of M31 (Ibata et al. 2007) have revealed a similarly rich set of substructure in the stellar halo of that galaxy. Based on photometry of main sequence turn-off (MSTO) stars, B08 constructed a coarse 3D map of the stellar halo density, with almost a factor of two uncertainty in distances. BHB stars are a much rarer tracer of the old metal-poor population, but have the great advantage of being luminous, with $M_g \sim +0.7$ (vs. $M_g \sim 3.5$ for MSTO stars) and of having precise distance estimates ($\sim 5\%$; X08). BHB stars have also been a special spectroscopic target class in SDSS and SEGUE (e.g., Yanny et al. 2009b). Hence, the sample of possible BHB stars with spectra from SDSS constitutes by far the largest set of luminous tracers (extending to distances of ~ 80 kpc) of the Milky Way’s stellar halo with available four dimensional ($\alpha, \delta, d, V_{los}$) information, where the distances are accurate to 5%

and the radial velocities accurate to $5 \sim 20 \text{ km s}^{-1}$. This sample enables the first attempt at checking that the statistical properties of kinematics matches (or not) model expectation.

This paper presents a large sample of probable BHB stars with measured kinematics, and it presents an exploration of how to quantify position-velocity substructure in the Milky Way’s stellar halo, in order to compare the observation to simulations such as from BJ05. It is certainly possible to pick out the kinematic signature of the Sagittarius stream (e.g., Ibata et al. 2001; Starkenburg et al. 2009) in these data. However, what we aim for here is to devise a simple objective measure for quantifying such substructure. Specifically, we employ the close pair distribution (CPD) statistic, $F = w_\theta \theta^2 + w_{\Delta d} (\Delta d)^2 + w_{\Delta V_{los}} (\Delta V_{los})^2$, to detect substructure, following Starkenburg et al. (2009). Here, θ , Δd , ΔV_{los} are the angular, distance, and velocity separation of pairs of stars, and w_θ , $w_{\Delta d}$, and $w_{\Delta V_{los}}$ are suitable weights. The idea is that a structured or “clumpy” position-velocity distribution will have more pairs with small F than a suitably chosen random distribution. As also argued by B08, it is important for quantitative data-model comparisons to have a general statistical measure of substructure, rather than specifically searching for (here, kinematical) substructure associated with a particular feature, such as the Sagittarius stream, so we also explore what we should expect from the BJ05 models, and compare with the observations.

This paper is organized as follows. In Section 2 we present the sample of BHB stars. Section 3 provides the definition of the close pair distribution (CPD) as a statistic, and describes its application to the sample of BHB stars. The analogous CPD for the BJ05 simulations and their statistical analysis is presented in Section 4. Conclusions from the comparisons between observations and simulations are presented in Section 5.

2. The Spectroscopic Sample of BHB stars from SDSS DR8

SDSS-I was an imaging and spectroscopic survey that began routine operations in April 2000, and continued through June 2005. The SDSS and its extensions are using a dedicated 2.5m telescope (Gunn et al. 2006) located at the Apache Point Observatory in New Mexico. The Sloan Extension for Galactic Understanding and Exploration (SEGUE) is one of the three key projects (the legacy survey, the supernova survey, and SEGUE) in the recently completed first extension of the Sloan Digital Sky Survey, known collectively as SDSS-II. The SEGUE program, which ran from July 2005 to July 2008, obtained *ugriz* imaging of some 3500 deg^2 of sky outside of the SDSS-I footprint (Fukugita et al. 1996; Gunn et al. 1998, 2006; York et al. 2000; Hogg et al. 2001; Smith et al. 2002; Stoughton et al. 2002; Abazajian et al. 2003, 2004, 2005, 2009; Pier et al. 2003; Ivezić et al. 2004; Adelman-McCarthy et al. 2006, 2007, 2008; Tucker et al. 2006), with special attention being given to scans of lower Galactic

latitudes ($|b| < 35^\circ$) in order to better probe the disk/halo interface of the Milky Way. SEGUE obtained some 240,000 medium-resolution spectra of stars in the Galaxy, selected to explore the nature of stellar populations from 0.5 kpc to 100 kpc (Yanny et al. 2009b). SDSS-III, which is presently underway, has already completed the sub-survey SEGUE-2, an extension intended to obtain an additional sample of over 120,000 spectra for distant stars that are likely to be members of the outer-halo population of the Galaxy. Data from SEGUE-2 will be distributed as part of the next public data release, DR8.

The SEGUE Stellar Parameter Pipeline processes the wavelength- and flux-calibrated spectra generated by the standard SDSS spectroscopic reduction pipeline (Stoughton et al. 2002), obtains equivalent widths and/or line indices for more than 80 atomic or molecular absorption lines, and estimates T_{eff} , $\log g$, and $[\text{Fe}/\text{H}]$ through the application of a number of approaches (see Lee et al. 2008a,b; Allende Prieto et al. 2008; Smolinski et al. 2010).

We construct a sample of BHB stars from SDSS DR8 with spectra in a fashion very similar to X08. The spectra are used both to classify stars as BHB and to obtain measured radial velocities. In essence, we combine an initial color cut for BHB candidates with Balmer-line profile shape measurements. The S/N of the spectra affects the precision of Balmer-line profile shape measurements. Therefore, spectra are only accepted when the fractional variance between the best-fitting profile and observed Balmer-line profile is ≤ 0.1 . The color cuts that we used in this paper are:

$$\begin{aligned} 0.8 < u - g < 1.5 \\ -0.5 < g - r < 0.0 \end{aligned}$$

The Balmer-line profile cuts used are:

$$\text{for the H}\delta \text{ line :} \quad D_{0.2} \leq 29 \text{ \AA}, \quad f_m \leq 0.35$$

$$\text{for the H}\gamma \text{ line :} \quad 0.75 \leq c_\gamma \leq 1.25, \quad 7 \text{ \AA} \leq b_\gamma \leq 10.8 - 26.5 (c_\gamma - 1.08)^2$$

where $D_{0.2}$, f_m , c , and b are the width of the Balmer line at 20% below the local continuum, the flux relative to the continuum at the line core, and the parameters of the Sérsic profile, $y = 1.0 - a \exp \left[- \left(\frac{|\lambda - \lambda_0|}{b} \right)^c \right]$, respectively (see Sirko et al. 2004, X08).

The following are the Balmer-line profile cuts used in X08:

$$\text{for the H}\delta \text{ line :} \quad 17 \text{ \AA} \leq D_{0.2} \leq 28.5 \text{ \AA}, \quad 0.1 \leq f_m \leq 0.3$$

$$\text{for the H}\gamma \text{ line :} \quad 0.75 \leq c_\gamma \leq 1.25, \quad 7 \text{ \AA} \leq b_\gamma \leq 10.8 - 26.5 (c_\gamma - 1.08)^2$$

We retain the color cut (Yanny et al. 2000), but slightly relax the Balmer-line profile cuts compared to X08, as illustrated in Figure 1. Since the two Balmer-line profile cuts are independent, the relaxed criteria on the $H\delta$ line should introduce little additional contamination, but overall it makes the criteria less stringent. As compared with our previous criteria (X08), the relaxed criteria will have minimal impact on the following substructure analysis. For further details on the sample selection, we refer the interested reader to X08 and references therein.

By selecting stars that satisfy the color cuts and both Balmer-line profile cuts, we obtain a sample of 4985 stars from SDSS DR8 with high BHB probability, of which there are 4651 halo BHB stars with $|Z| > 4$ kpc and $r_{\text{gc}} < 80$ kpc. Figure 2 shows the sky coverage and spatial distribution of these 4651 halo BHB stars, along with the cumulative distribution of their distance to the Galactic center and their line-of-sight velocity distribution. Distances were derived from the magnitudes and colors as in X08. The line-of-sight velocities, V_{los} , are converted from Local Standard of Rest frame to the Galactic Standard of Rest frame by adopting a value of 220 km s^{-1} for the Local Standard of Rest (V_{lsr}) and a solar motion of $(+10.0, +5.2, +7.2) \text{ km s}^{-1}$, as in X08. Small changes that may arise from adopting a different $V_{\text{cir}}(R_0)$ pair, e.g., Bovy et al. (2009) or Koposov et al. (2010), do not matter for the subsequent analysis.

This sample of halo BHB stars has radial velocity errors of $5\text{-}20 \text{ km s}^{-1}$ and much more accurate distances than other distant halo stars with available kinematic information. For instance, distances are $\sim 4\times$ more accurate than in the sample of halo giants recently used by Starkenburg et al. (2009) in a search for distant halo substructure, and our sample is 50-fold larger. Schlafman et al. (2009) discussed a sample of $\sim 10,000$ metal-poor main sequence turnoff (MPMSTO) stars with distances greater than 10 kpc from the Galactic center, with vertical distance $|Z|$ more than 4 kpc, and with distances less than 17.5 kpc from the Sun, to identify ECHOS in the inner halo. By comparison, our sample extends to four times larger distances.

The cumulative distribution of the BHB stars with r shown in Figure 2 indicates that about 95% of the BHB stars have $r_{\text{gc}} \leq 40$ kpc, so that any estimate of substructure should be dominated by the BHB stars within this distance. For a cleaner selection function, we use only the 4243 BHB stars with $|Z| > 4$ kpc and $r_{\text{gc}} \leq 40$ kpc in the following analysis, which is still sufficiently distant to enable tests for substructure well into the outer halo.

3. The Close Pair Distribution of BHB stars in DR8

We now turn to quantifying the presence of any kinematic substructure. There is no unique choice of a substructure statistic, nor is there a rigorous way to derive one without making very specific assumptions about the nature of the underlying distributions. For kinematically cold streams that are not strongly phase mixed, a “pairwise velocity difference” (PVD), $\langle |\Delta V_{los}| \rangle (\Delta r_{gc}^{\vec{r}})$, could conceivably be used to detect velocity substructure. It is expected that $\langle |\Delta V_{los}| \rangle$ should be lower for small separations $\Delta r_{gc}^{\vec{r}}$ in stellar streams, where adjacent stars have similar velocities. However, as many streams in simulated halos are phase wrapped, the PVD proved not to be very suitable to quantify substructure, even in simulated halos where all stars arise from disrupted satellites (see Xue et al. 2009).

As an alternative to the PVD, we follow Starckenburg et al. (2009) and De Propriis et al. (2010) in exploring a statistic that focuses on the incidence of close pairs in $(\alpha, \delta, d, V_{los})$ space (similar to the approach of Doinidis & Beers 1989). Specifically, we define the separation between two stars i and j as:

$$F_{ij} = w_{\theta} \theta_{ij}^2 + w_{\Delta d} (d_i - d_j)^2 + w_{\Delta V_{los}} (V_{los,i} - V_{los,j})^2 \quad (1)$$

where

$$\cos \theta_{ij} = \cos b_i \cos b_j \cos(l_i - l_j) + \sin b_i \sin b_j,$$

$$w_{\theta} = \frac{1}{\langle \theta^2 \rangle}, w_{\Delta d} = \frac{1}{\langle (\Delta d)^2 \rangle}, w_{\Delta V_{los}} = \frac{1}{\langle (\Delta V_{los})^2 \rangle};$$

and where $\langle \dots \rangle$ refers to the average over all pairs.

If position-velocity substructure is present, we expect that the distribution of F_{ij} for the observed sample has more close pairs than the null hypothesis (defined below) of a smooth halo where positions and velocities are uncorrelated: $N_{obs}(\langle F \rangle) > N(\langle F_0 \rangle)$. This is most conveniently captured in the cumulative distribution of the F_{ij} , $N(\langle F \rangle)$, as illustrated in Figure 3.

This null hypothesis assumes that the halo can be described by some spatial density distribution, $\rho_{BHB}(\vec{r})$, and a velocity distribution where σ_{los} does not depend on the particular position. Indeed, averaged over all angles, $\sigma_{los} \approx 111 \text{ km s}^{-1}$ is observed to be nearly constant as a function of radius (X08). In its angular distribution and its distance distribution, the sample selection function of our BHB sample is very complex (see, e.g., Figure 2 for the angular distribution). However, stellar radial velocities are uncorrelated to the sample selection, and it is reasonable to assume that the distance selection of the stars in the same part of the sky are independent realizations of the overall distance (or, apparent magnitude)

distribution. Consequently, we cannot randomize θ when constructing the null hypotheses. As our null hypothesis, we can only independently draw random Δd and ΔV_{los} . Specifically, we do this by scrambling *only* the distances and velocities within the sample to create the null hypothesis, but leave the angular position unchanged:

$$F_{0,ij} = w_\theta \theta_{ij}^2 + w_d (d_{i_r} - d_{j_r})^2 + w_{V_{los}} (V_{los,i_r} - V_{los,j_r})^2, \quad (2)$$

where $w_\theta, w_d, w_{V_{los}}$, and the indices i and j are exactly the same as in F_{ij} , but i_r and j_r are random indices chosen within an angle¹ of 45° from stars i and j (here, i_r and j_r are different and independent in their distance and velocity terms).

Now we can search for position-velocity substructure by comparing $N_{obs}(< F)$ for our BHB sample to the distribution of 100 Monte Carlo representations of $N(< F_0)$. Figure 3 shows that $N_{obs}(< F)$ exceeds $N(< F_0)$ at high significance for small F , $\log F < -2$ (for example, $\Delta d < 1.5$ kpc, $\Delta V_{los} < 15$ km s⁻¹ and $\theta < 8^\circ$ corresponds to $\log F < -2$).

Small values of F represent close pairs in position-velocity space. So, Figure 3 demonstrates that the observed sample has many more close pairs than the null hypothesis, reflecting the existence of position-velocity substructure in the BHB sample. For small F one might expect $N(< F_0) \propto F_0^2$ for the null hypothesis, but the plot shows a somewhat shallower slope, presumably arising from the non-random way that stars are sampled by SDSS spectroscopy from the celestial sphere. The widely spaced SEGUE-1/2 spectroscopic plates result in the sparse, but locally dense, angular sampling. In addition, we can learn from Figure 3 that the CPD statistic focuses on $< 0.1\%$ close pairs rather than all pairs of the sample, implying that the CPD may be more sensitive to the presence of substructure than the PVD statistic (see Xue et al. 2009).

As shown in Figure 4, the substructure signal comes both from the distance and the line-of-sight velocity domain. This is apparent if we either scramble *only* the distances (upper panel) or *only* the velocities (lower panel) between $N_{obs}(< F)$ and $N(< F_0)$. In both cases an excess of small separation pairs is present at a comparable level.

The recent studies of Carollo et al. (2007) and Carollo et al. (2010), based on local samples of halo stars, indicate that our Milky Way’s stellar halo is complex, and can be described by at least two components – denoted as an “inner” and an “outer” halo, with different kinematics, distributions of orbital eccentricity, inferred spatial profiles, and peak

¹Angular spacing comparable to or larger than the SDSS footprint may be hard to interpret, so we choose 45° to avoid this.

metallicities. In such a decomposition, the inner halo component dominates the region of $5 \text{ kpc} < r_{\text{gc}} < 10 \text{ kpc}$, while the region $r_{\text{gc}} > 10 \text{ kpc}$ is dominated by the outer halo. Direct in situ evidence for stellar metallicity changes with distance has also been found in photometry from the SEGUE vertical stripes (de Jong et al. 2010).

As dynamical timescales are longer at large distances, we would expect a more clear substructure signal in the outer parts of the halo. To test this, we re-introduce the BHB stars with $40 \text{ kpc} < r_{\text{gc}} < 60 \text{ kpc}$. Though this portion of the BHB sample does not contribute much to the signal of the whole BHB sample, it is important to test how the signals change with distance. We divide the BHB sample into three parts – subsample I with $5 \text{ kpc} < r_{\text{gc}} < 10 \text{ kpc}$, subsample II with $10 \text{ kpc} < r_{\text{gc}} < 40 \text{ kpc}$, and subsample III with $40 \text{ kpc} < r_{\text{gc}} < 60 \text{ kpc}$, all with $|Z| > 4 \text{ kpc}$, and compare the substructure signals in all subsamples. Figure 5 shows that all three show significant deviations from the null hypothesis. The Figure also shows that the statistical significance of the signal is stronger in the outer halo (subsample II, III) than in the inner halo (subsample I). Note that the actual level of $N(< F)$ in Figure 5 depends on the projected sky density of BHB stars as a function of their distance, so the $N(< F)$ for subsample II appears higher than the other subsamples (see also Figure 9).

As mentioned in the introduction, we are more interested in a general statistical measure of substructure for quantitative data-model comparison than in the search for substructure associated with a particular feature; $N(< F)$ appears as a useful statistic in this context.

4. Position-Velocity Substructure in the BJ05 Models

Having detected a general substructure signal, we now compare this to expectations for $N(< F)$ from cosmological models where the entire stellar halo is made of disrupted satellite galaxies.

BJ05 published models for the formation of the stellar halo of the Milky Way system, arising solely from the accretion of $\sim 100 - 200$ luminous satellite galaxies in the past ~ 12 Gyr. They used a hybrid semi-analytic plus N-body approach that distinguished explicitly between the evolution of baryonic matter and dark matter in accreted satellites. For further details of the simulations, we refer the interested reader to BJ05 and references therein. There are 11 simulated halos provided by the Bullock & Johnston study. The simulations produce a realistic stellar halo, with mass and density profiles much like that of the Milky Way (e.g. B08), and with surviving satellites matching the observed number counts and structural parameter distributions of the satellite galaxies of the Milky Way.

To start, we assume that BHB stars are representative tracers of the overall population of old, metal-poor, halo stars (see, however, Bell et al. 2010). We then make “mock-observations” of the BJ05 simulations, analogous to those presented in Section 2 and analyzed in Section 3. In brief, we do this by accounting for the particular survey volume of SDSS DR8, the angular separation distribution, and approximate distance distribution of the BHB sample, accounting for the luminosity weight of the simulated particles, and by adding observational uncertainties for distance and velocity.

From the simulations, we obtain the particle’s 3D positions and 3D velocities in the Galactic standard of rest frame, luminosities L , and ages. We transfer these to Galactocentric line-of-sight velocities, V_{los} , and sky positions (Galactic longitude and latitude, (l, b)), by taking the Sun’s position as $(8.0, 0.0)$ kpc. The probability of a particle being drawn is proportional to the assigned particle luminosity. We also consider the spectroscopic sky coverage of SDSS DR8, distance limits ($|Z| \geq 4$ kpc, $r_{gc} \leq 40$ kpc), and the angular separation distribution of the observations. These procedures essentially follow those used by X08.

Based on the particles with the same sky coverage as SDSS DR8 and the same distance limits as the BHB sample, we randomly select a particle within an angle² of 1.2° from each BHB star i in the sample (where $i = 1 \dots 4243$). This selected particle of luminosity L is accepted with a probability of $\leq L/L_{max}$, where L_{max} is the maximum luminosity of the simulated particles. We also convolve the distances of the mock-observations with an error of 5%; the radial velocities are convolved with a Gaussian error of $\sigma = 5$ km s⁻¹.

This procedure results in mock-observations of 4243 star particles in the simulations that are in the same sky region as SDSS DR8, have a similar angular separation distribution to the BHB sample, have the same distance and velocity uncertainties as the BHB sample, and have distance limits of $|Z| \geq 4$ kpc, $r_{gc} \leq 40$ kpc, and satisfy the luminosity weighting scheme. These mock-observations allow us to consider the CPD for the BJ05 simulations. We calculate F for the mock-observations and 100 sets of the null hypothesis, F_0 , in each of the 11 simulations.

The CPDs of the mock-observations for all 11 simulated halos of BJ05 are shown in Figure 6, along with the CPD of the actual data in the top left panel. Inspection of this Figure reveals that $N_{obs}(< F)$ differs significantly from $N(< F_0)$ for all halos, in the sense that $N_{obs}(< F) > N(< F_0)$ at least for $< 1\%$ of closest pairs. The strength of the CPD signature varies quite strongly among different simulations (e.g., halo12 *vs.* halo15 in Figure 6). Overall, the ensemble of simulations show qualitatively the same signature of position-velocity

²The 1.2° angular distance was found to be the smallest angle that can ensure there is at least one particle that can be accepted around star i .

substructure as seen in the real data. Moreover, the strength of the signal for $\log F < -2$ in the observations lies within the range of the simulations, while the simulations exhibit stronger signals than observation for $-2 < \log F < -1$ (Figure 7). In particular, a significant substructure signal can be traced in the mock-observations to $\log F \sim -1$ (e.g., $\Delta d < 4.5$ kpc, $\Delta V_{los} < 65$ km s⁻¹, and $\theta < 26^\circ$ for $\log F < -1$) for most of the simulations (except halo07 and halo15), while for the observations the substructure signal can only be traced until $\log F \sim -2$. This indicates some quantitative data-model difference.

To explore why the models might be somewhat more highly structured especially for larger F , we carry out two tests. First we focus on the CPDs only on smaller angular scales, by only considering $\theta < 10^\circ$. For most simulations, CPDs with $\theta < 10^\circ$ exhibit substructure signals that still can be traced beyond $\log F \sim -2$; in the BHB sample the substructure signals can be traced only for $\log F < -2$. Therefore, the angular distance distribution is not the dominant cause of the data-model difference for $-2 < \log F < -1$.

Second, we compare the F distributions for the observation and the particles older than 11 Gyr in the BJ05 halos, where the age refers to the formation of the star particle, not the time since disruption of its host satellite. Figure 8 shows that the observed substructure signal is comparable with those detected in simulations (except for halo02 and halo12). BHB stars are known to represent a very old population, so this may be an astrophysically sensible reason for the data-model difference.

Another possibility is that, since the models do not follow mergers self-consistently (i.e., the Milky Way’s potential grows only smoothly and analytically), the response of the Milky Way to infalling objects could serve to disrupt and scatter streams, thereby decreasing the importance of substructure. This could be checked in the future with simulations such as Cooper et al. (2010).

As in the analysis of the BHB sample, we also make mock observations of the inner- and outer-halo regions (here, the mock observations have similar sky densities to the BHB sample), and calculate F and F_0 for the mock observations. Figure 9 shows that, for most BJ05 halos (except halo07 and halo15), the outer halo exhibits a stronger substructure signal than the inner halo, but the actual level of $N(< F)$ depends on the projected sky density of particles as a function of their distance, consistent with the observations in the top left panel.

The mock-observations show that the CPD deviates from the null hypothesis in the simulations in a qualitatively similar fashion as the actual observations. At first sight, this seems to be a straightforward extension into the kinematic domain of the conclusion reached by B08, that the stellar halo exhibits a level of substructure consistent with the stream-only

models of BJ05.³ The signal is, however, weaker than that seen in mock-observations drawn from the BJ05 simulations.

Taken together, Figure 3, Figure 5, Figure 6, Figure 8 and Figure 9 lead to our four results: 1) In a sample of > 4000 BHB stars from SDSS DR8 there is a very clear signal for position-velocity substructure in the Milky Way’s halo stars – close angular pairs of stars have smaller velocity and/or distance differences than expected for an uncorrelated distribution. 2) The outer part of the Milky Way’s halo ($r_{gc} > 10$ kpc) exhibits a statistically stronger kinematic substructure signal than the inner halo ($r_{gc} \leq 10$ kpc). 3) Mock-observations of simulated halos BJ05 made exclusively from disrupted satellites, exhibit a qualitatively very similar behavior – $N_{\text{obs}}(< F) > N(< F_0)$ for $\log F \leq -1$. 4) Quantitatively, most simulations produce a stronger signal, especially one extending to larger scales (i.e., larger F). However, if we identify BHB stars with the simulated halo population with $t_{age} > 11$ Gyr, the levels of substructure are consistent. Given other evidence that BHB stars are most abundant in very old populations, this seems perhaps astrophysically more plausible than the alternative of postulating a very quiet formation of the Milky Way’s halo.

5. Summary and Conclusions

In the context of current cosmogonic models, the stellar halos of galaxies like our Milky Way are expected to be comprised, to a large degree, of debris from disrupted satellite galaxies. After disruption, the dispersing stars will form recognizable streams for some time, but may eventually phase-mix beyond easy recognition. There has been recent evidence (B08) that the degree of spatial substructure actually seen in the Milky Way’s halo matches that of simulations (e.g., BJ05), where the stellar halo arises exclusively from disrupted satellites. Due to phase-space conservation, the same scenario qualitatively predicts the existence of a position-velocity correlation. In this paper, we have pursued a quantitative statistical approach to understanding how the Milky Way’s stellar halo compares with this scenario.

It has already been established in the published literature that several prominent substructures exist in the Milky Way’s stellar halo, most notably the Sagittarius stream. The next step forward is to find simple, robust statistical measures to quantify the level of substructure in order to allow direct comparison with theoretical models (such as BJ05). There is certainly no established procedure, and there may be no unique way to establish such a

³In Bell et al. (2008) the BJ05 models are labeled 1-11 in strict numerical order, so that the interested reader can compare B08 and this paper side-by-side.

statistic. For example, in pure position space, B08 simply took the *rms* deviation of the density from a underlying power-law model. In this paper we have considered a statistic for diagnosing position-velocity correlations – the close pair distribution (see Starkenburg et al. 2009).

Building on recent initial attempts (Starkenburg et al. 2009; Xue et al. 2009; Harrigan et al. 2010; De Propris et al. 2010), this paper presented a more comprehensive attempt to quantify the position-velocity substructure of the Milky Way’s stellar halo, using BHB stars from SDSS, and to compare it to cosmological models. We calculated the close pair distribution (CPD) as a function of distance separation, angular separation, and velocity separation between pairs of stars. Qualitatively, the signal we were looking for is that the observations have significantly more close pairs than an ensemble of null hypotheses, where the position and velocity have no correlation. Using this CPD (i.e., the cumulative distribution $N_{\text{obs}}(< F)$, where F is the four-distance in angle, distance, and velocity), we found that a sample of over 4000 BHB stars in the halo of the Galaxy exhibit far more close pairs than the null hypothesis, which demonstrates the existence of real substructure. This result is perhaps not surprising, as some level of substructure is already known to exist (see also Starkenburg et al. 2009; De Propris et al. 2010; Harrigan et al. 2010). However, as a statistical quantification, it draws on a sample 6-60 times larger than previous analyses (Starkenburg et al. 2009; De Propris et al. 2010), and arrives at statistically very clear-cut inferences. We also constructed mock-observations of simulated stellar halos that are made exclusively of disrupted satellite galaxies. These mock-observations match the angular sampling of the SDSS data in detail, and also match the distance cuts applied to the data. Comparing, analogously, $N_{\text{obs}}(< F)$ to $N(< F_0)$, we found the qualitatively same signature of substructure as in the observed sample. Quantitatively, the observed signal is weaker than that seen in the mock-observations, where the stellar halo is entirely made of disrupted satellites. Assuming that BHB stars are random tracers of the stars in the simulations, we impose a lower age limit of 11 Gyr in producing mock observations, and found consistent levels of position-velocity substructure between observation and simulations. Therefore, there are two ways to reconcile the data-model differences: either to infer differences in the dynamical formation histories between the simulated and the observed Milky Way, or - more plausible in our view - attributing it to the fact that BHB stars are overrepresented in the oldest sub-populations of the stellar halo. For both the observations and the mock-observations we compared the substructure signals associated with the inner and outer halos, and found good agreement between data and model – the outer halo exhibits a stronger substructure signal than the inner halo.

Within the context of SDSS data, the next level of understanding kinematic substructure in the Milky Way’s outer halo will come from samples of more representative giant stars with

good distances. How the results from BHB stars presented here relate to the substructure seen in main-sequence samples of the inner halo (Schlaufman et al. 2009, ECHOS) remains to be resolved. A more recent generation of simulations (e.g. Cooper et al. 2010) will also permit more far reaching and robust conclusions.

Funding for SDSS-III has been provided by the Alfred P. Sloan Foundation, the Participating Institutions, the National Science Foundation, and the U.S. Department of Energy. The SDSS-III web site is <http://www.sdss3.org/>.

SDSS-III is managed by the Astrophysical Research Consortium for the Participating Institutions of the SDSS-III Collaboration including the University of Arizona, the Brazilian Participation Group, Brookhaven National Laboratory, University of Cambridge, University of Florida, the French Participation Group, the German Participation Group, the Instituto de Astrofísica de Canarias, the Michigan State/Notre Dame/JINA Participation Group, Johns Hopkins University, Lawrence Berkeley National Laboratory, Max Planck Institute for Astrophysics, New Mexico State University, New York University, the Ohio State University, University of Portsmouth, Princeton University, University of Tokyo, the University of Utah, Vanderbilt University, University of Virginia, University of Washington, and Yale University.

This work was made possible by the support of the Max-Planck-Institute for Astronomy, and was funded by the National Natural Science Foundation of China (NSFC) under Nos. 10821061, 10876040 and 10973021. This work was also supported by the National Basic Research Program of China under grant 2007CB815103.

E. F. B. acknowledges NSF grant AST 1008342.

T.C.B. and Y.S.L. acknowledge partial funding of this work from grants PHY 02-16783 and PHY 08-22648: Physics Frontier Center/Joint Institute for Nuclear Astrophysics (JINA), awarded by the U.S. National Science Foundation.

H. Morrison acknowledges funding of this work from NSF grant AST-0098435.

REFERENCES

- Abazajian, K., Adelman-McCarthy, J. K., Agüeros, M. A., et al. 2004, *AJ*, 128, 502
Abazajian, K., Adelman-McCarthy, J. K., Agüeros, M. A., et al. 2005, *AJ*, 129, 1755
Abazajian, K., Adelman-McCarthy, J. K., Agüeros, M. A., et al. 2003, *AJ*, 126, 2081
Abazajian, K. N., Adelman-McCarthy, J. K., Agüeros, M. A., et al. 2009, *ApJS*, 182, 543

- Adelman-McCarthy, J. K., Agüeros, M. A., Allam, S. S., et al. 2008, *ApJS*, 175, 297
- Adelman-McCarthy, J. K., Agüeros, M. A., Allam, S. S., et al. 2007, *ApJS*, 172, 634
- Adelman-McCarthy, J. K., Agüeros, M. A., Allam, S. S., et al. 2006, *ApJS*, 162, 38
- Allende Prieto, C., Sivarani, T., Beers, T. C., et al. 2008, *AJ*, 136, 2070
- Bell, E. F., Xue, X., Rix, H., Ruhland, C., & Hogg, D. W. 2010, *AJ*, accepted
- Bell, E. F., Zucker, D. B., Belokurov, V., et al. 2008, *ApJ*, 680, 295 [B08]
- Blumenthal, G. R., Faber, S. M., Primack, J. R., & Rees, M. J. 1984, *Nature*, 311, 517
- Bovy, J., Hogg, D. W., & Rix, H. 2009, *ApJ*, 704, 1704
- Carollo, D., Beers, T. C., Chiba, M., et al. 2010, *ApJ*, 712, 692
- Carollo, D., Beers, T. C., Lee, Y. S., et al. 2007, *Nature*, 450, 1020
- Cooper, A. P., Cole, S., Frenk, C. S., et al. 2010, *MNRAS*, 406, 744
- de Jong, J. T. A., Yanny, B., Rix, H., et al. 2010, *ApJ*, 714, 663
- De Propris, R., Harrison, C. D., & Mares, P. J. 2010, *ApJ*, 719, 1582
- Dehnen, W. & Binney, J. J. 1998, *MNRAS*, 298, 387
- Doinidis, S. P. & Beers, T. C. 1989, *ApJ*, 340, L57
- Fukugita, M., Ichikawa, T., Gunn, J. E., et al. 1996, *AJ*, 111, 1748
- Gunn, J. E., Carr, M., Rockosi, C., et al. 1998, *AJ*, 116, 3040
- Gunn, J. E., Siegmund, W. A., Mannery, E. J., et al. 2006, *AJ*, 131, 2332
- Harrigan, M. J., Newberg, H. J., Newberg, L. A., et al. 2010, *MNRAS*, 405, 1796
- Helmi, A., White, S. D. M., de Zeeuw, P. T., & Zhao, H. 1999, *Nature*, 402, 53
- Hogg, D. W., Finkbeiner, D. P., Schlegel, D. J., & Gunn, J. E. 2001, *AJ*, 122, 2129
- Ibata, R., Lewis, G. F., Irwin, M., Totten, E., & Quinn, T. 2001, *ApJ*, 551, 294
- Ibata, R., Martin, N. F., Irwin, M., et al. 2007, *ApJ*, 671, 1591
- Ibata, R. A., Gilmore, G., & Irwin, M. J. 1994, *Nature*, 370, 194

- Ibata, R. A., Gilmore, G., & Irwin, M. J. 1995, *MNRAS*, 277, 781
- Ivezić, Ž., Goldston, J., Finlator, K., et al. 2000, *AJ*, 120, 963
- Ivezić, Ž., Lupton, R. H., Schlegel, D., et al. 2004, *Astronomische Nachrichten*, 325, 583
- Klement, R., Fuchs, B., & Rix, H. 2008, *ApJ*, 685, 261
- Klement, R., Rix, H., Flynn, C., et al. 2009, *ApJ*, 698, 865
- Koposov, S. E., Rix, H., & Hogg, D. W. 2010, *ApJ*, 712, 260
- Lee, Y. S., Beers, T. C., Sivarani, T., et al. 2008a, *AJ*, 136, 2022
- Lee, Y. S., Beers, T. C., Sivarani, T., et al. 2008b, *AJ*, 136, 2050
- Majewski, S. R., Munn, J. A., & Hawley, S. L. 1996, *ApJ*, 459, L73+
- Majewski, S. R., Skrutskie, M. F., Weinberg, M. D., & Ostheimer, J. C. 2003, *ApJ*, 599, 1082
- Morrison, H. L., Helmi, A., Sun, J., et al. 2009, *ApJ*, 694, 130
- Newberg, H. J., Yanny, B., Cole, N., et al. 2007, *ApJ*, 668, 221
- Newberg, H. J., Yanny, B., Rockosi, C., et al. 2002, *ApJ*, 569, 245
- Pier, J. R., Munn, J. A., Hindsley, R. B., et al. 2003, *AJ*, 125, 1559
- Schlaufman, K. C., Rockosi, C. M., Allende Prieto, C., et al. 2009, *ApJ*, 703, 2177
- Searle, L. & Zinn, R. 1978, *ApJ*, 225, 357
- Sirko, E., Goodman, J., Knapp, G. R., et al. 2004, *AJ*, 127, 899
- Skrutskie, M. F., Cutri, R. M., Stiening, R., et al. 2006, *AJ*, 131, 1163
- Smith, J. A., Tucker, D. L., Kent, S., et al. 2002, *AJ*, 123, 2121
- Smith, M. C., Evans, N. W., Belokurov, V., et al. 2009, *MNRAS*, 399, 1223
- Smolinski, J. P., Beers, T. C., Lee, Y. S., et al. 2010, *AJ*, submitted
- Starkenburger, E., Helmi, A., Morrison, H. L., et al. 2009, *ApJ*, 698, 567
- Stoughton, C., Lupton, R. H., Bernardi, M., et al. 2002, *AJ*, 123, 485

- Tucker, D. L., Kent, S., Richmond, M. W., et al. 2006, *Astronomische Nachrichten*, 327, 821
- White, S. D. M. & Rees, M. J. 1978, *MNRAS*, 183, 341
- Xue, X., Rix, H., & Zhao, G. 2009, *Research in Astronomy and Astrophysics*, 9, 1230
- Xue, X. X., Rix, H. W., Zhao, G., et al. 2008, *ApJ*, 684, 1143 [X08]
- Yanny, B., Newberg, H. J., Grebel, E. K., et al. 2003, *ApJ*, 588, 824
- Yanny, B., Newberg, H. J., Johnson, J. A., et al. 2009a, *ApJ*, 700, 1282
- Yanny, B., Newberg, H. J., Kent, S., et al. 2000, *ApJ*, 540, 825
- Yanny, B., Rockosi, C., Newberg, H. J., et al. 2009b, *AJ*, 137, 4377
- York, D. G., Adelman, J., Anderson, Jr., J. E., et al. 2000, *AJ*, 120, 1579

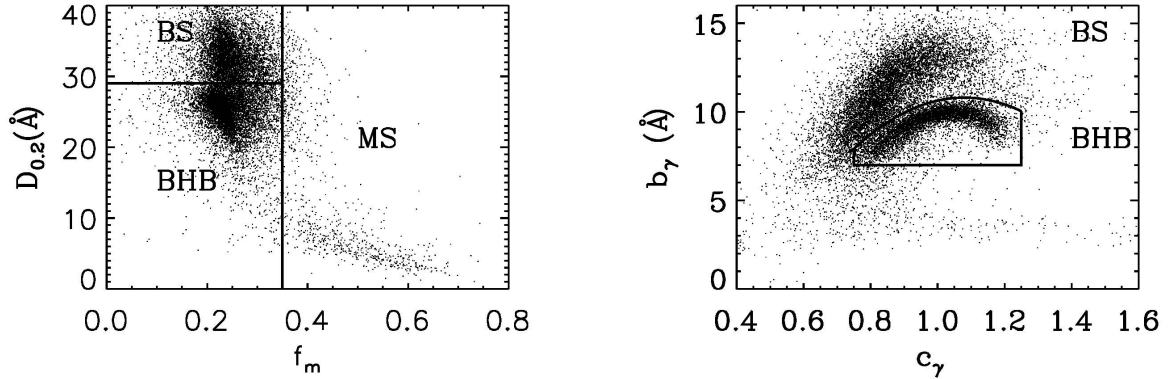


Fig. 1.— BHB star sample selection, based on the Balmer-line shape parameters (see Section 2). The left-hand panel shows the H δ line parameters f_m and $D_{0.2}$, divided into three regions (following X08 and Sirko et al. 2004): stars with $f_m > 0.35$ are too cool to be BHB stars – they are likely main-sequence stars; the concentration of stars with $D_{0.2} > 29\text{\AA}$ is likely due to blue stragglers (BS) with higher surface gravity; the region with $f_m \leq 0.35$ and $D_{0.2} \leq 29\text{\AA}$ is used as the BHB selection criterion for the H δ , $D_{0.2}$, and f_m method. The right-hand panel shows the H γ -line profile parameters c_γ and b_γ for the same stars as in the left panel. Here, BS and BHB stars can be distinguished clearly through their bimodal distribution in this plane. The enclosed region indicates the H γ scale width-shape criteria that selects BHB stars. Our BHB sample is composed of all stars satisfying both criteria (left-hand and right-hand panels) simultaneously. This leaves a sample of 4985 objects with a high probability of proper classification as BHB stars (see X08).

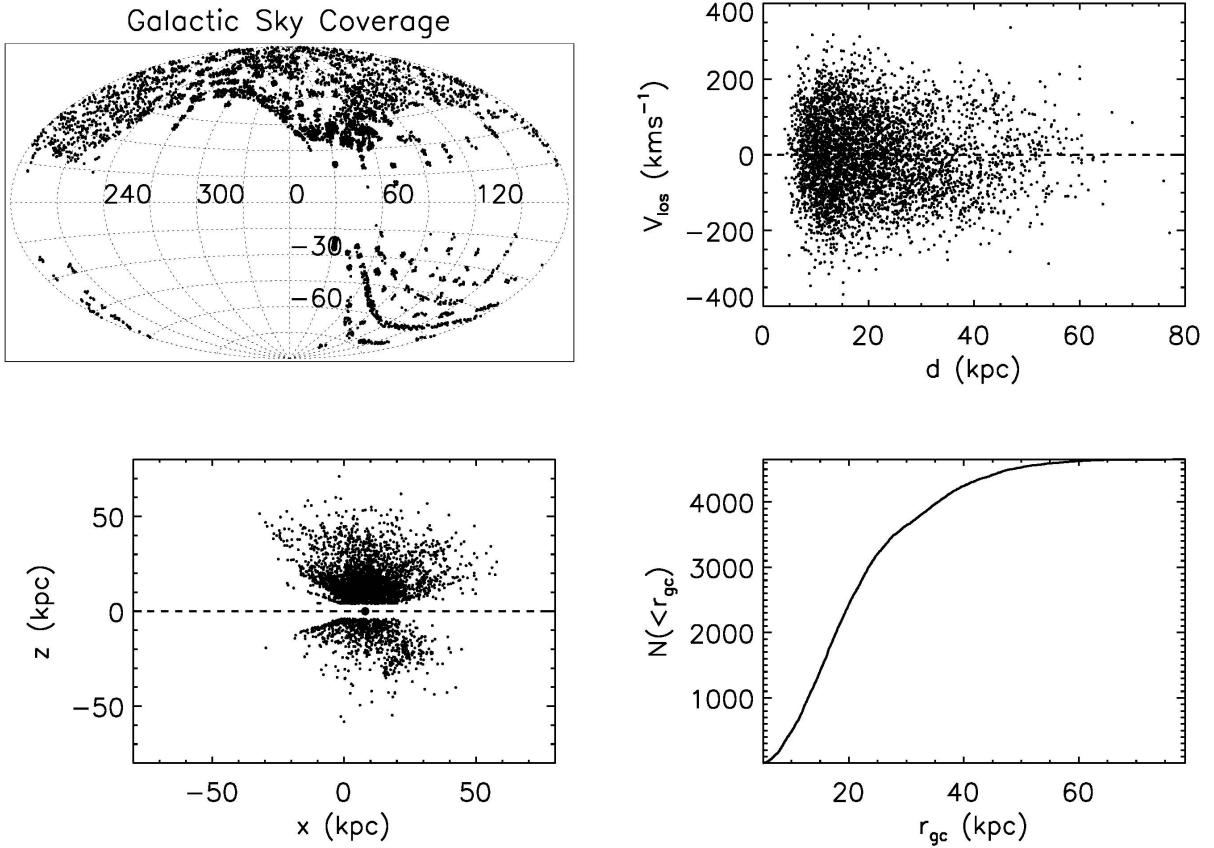


Fig. 2.— Sample properties for the 4985 stars with high probability of being BHB (Figure 1). The upper left-hand panel shows the sky coverage, and the lower left-hand panel shows the spatial distribution (x - z plane). The coordinate system has its origin at the Galactic center; the large filled circle on the x - z plot indicates the location of the Sun (8.0 kpc, 0 kpc). The upper right-hand panel shows the line-of-sight velocity distribution as a function of distance from the Sun d , while the lower right-hand panel is the cumulative distribution of BHB stars with distance from the Galactic center, r_{gc} (bottom), with a median distance of 22 kpc: about 90% of the sample lies between 5 kpc and 40 kpc.

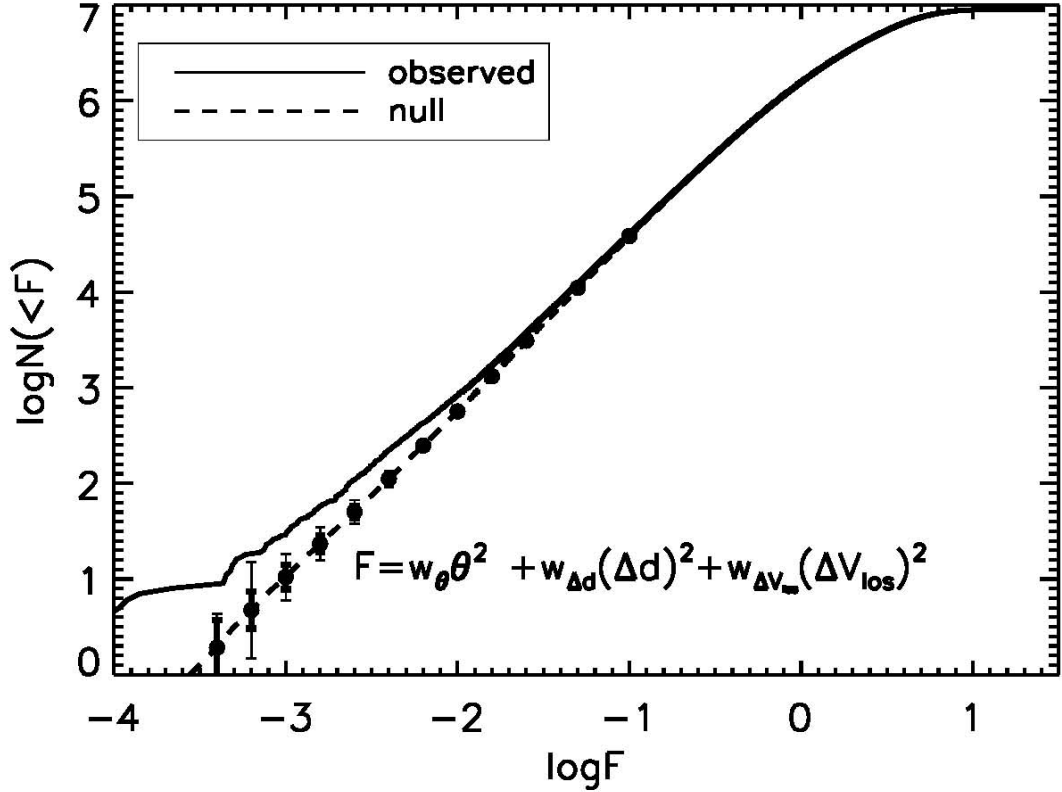


Fig. 3.— Close pair distribution, $N(< F)$, for the 4243 BHB stars in SDSS DR8 BHB sample with $|Z| > 4$ kpc and $r_{\text{gc}} < 40$ kpc. F is the four-space separation between two BHB stars, taking into account in angle, distance, and line-of-sight velocity (Eq. 1). The solid line is the cumulative distribution of F as observed; the dashed line is the average cumulative distribution of F for 100 null hypotheses, where positions, and hence, angular separations for each pair, were retained exactly as in the observations, but distances and line-of-sight velocities were scrambled (see Section 3). The filled circles denote the mean of 100 such null hypotheses; the thick error bars enclose 68% of the distribution, while the thin error bars enclose 95% of the null hypotheses. This plot demonstrates that there exists a significant excess of close pairs (in distance and velocity) compared to the null hypotheses: BHB stars in our sample clearly exhibit position-velocity substructure. For small F one might expect $N(< F_0) \propto F_0^2$, but the plot shows a somewhat shallower slope, presumably arising from the sparse, but locally dense, angular sampling that results from the widely spaced SEGUE-1/2 spectroscopic plates.

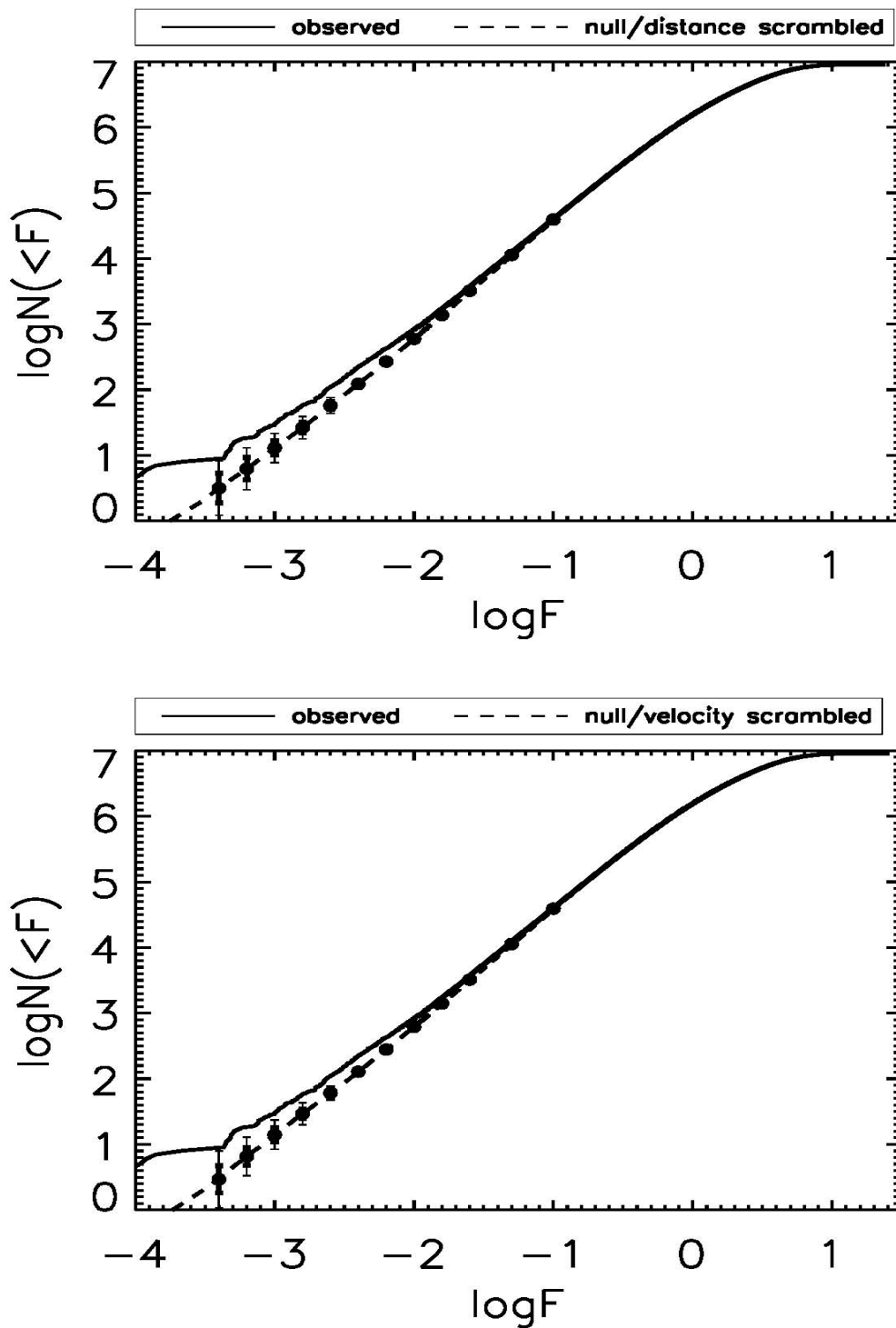


Fig. 4.— Close pair distribution for the BHB sample after either scrambling *only* the distances (upper panel), or *only* the velocities (lower panel). In both cases an excess of close pairs is observed at a comparable level. This implies that the substructure signal arises in comparable parts from both the distance and the line-of-sight velocity domains.

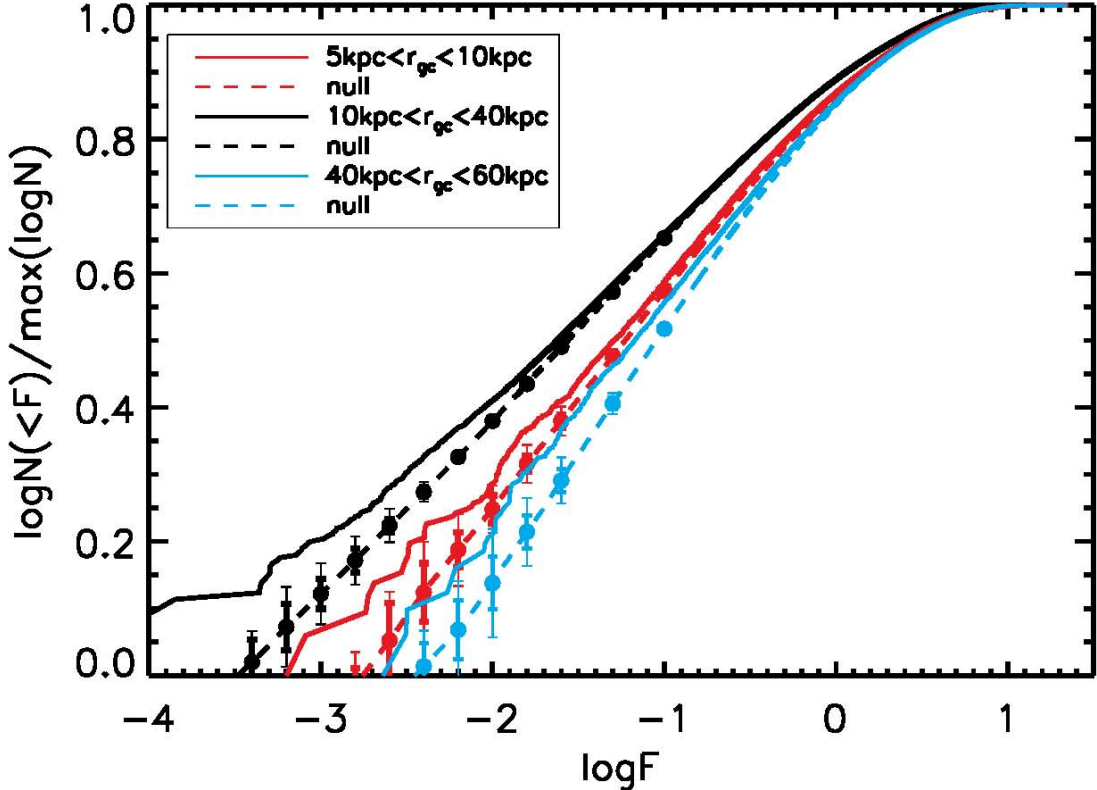


Fig. 5.— The close pair distribution of F for BHB stars in three broad Galactocentric distance ranges: Subsample I, which covers $5 \text{ kpc} < r_{\text{gc}} < 10 \text{ kpc}$ (red lines), Subsample II, which covers $10 \text{ kpc} < r_{\text{gc}} < 40 \text{ kpc}$ (black lines), and Subsample III, which covers $40 \text{ kpc} < r_{\text{gc}} < 60 \text{ kpc}$ (blue lines). The dashed lines are the corresponding average cumulative distributions of F for 100 null hypotheses as in Figure 3, for the respective subsamples. The filled circles locate the mean of the 100 null hypotheses; the thick error bars enclose 68% of the distribution, while the thin error bars enclose 95% of the null hypotheses. The figure shows that a position-velocity substructure signal is present in all distance ranges, covering the inner and outer stellar halo, but the actual level of $N(< F)$ depends on the projected sky density of BHB stars as a function of their distance. As seen in the lower right-hand panel of Figure 2, most BHB stars lie between 10 kpc and 40 kpc, so the $N(< F)$ for Subsample II is greater than those for Subsample I and II. However, the substructure signal is more pronounced at large radii.

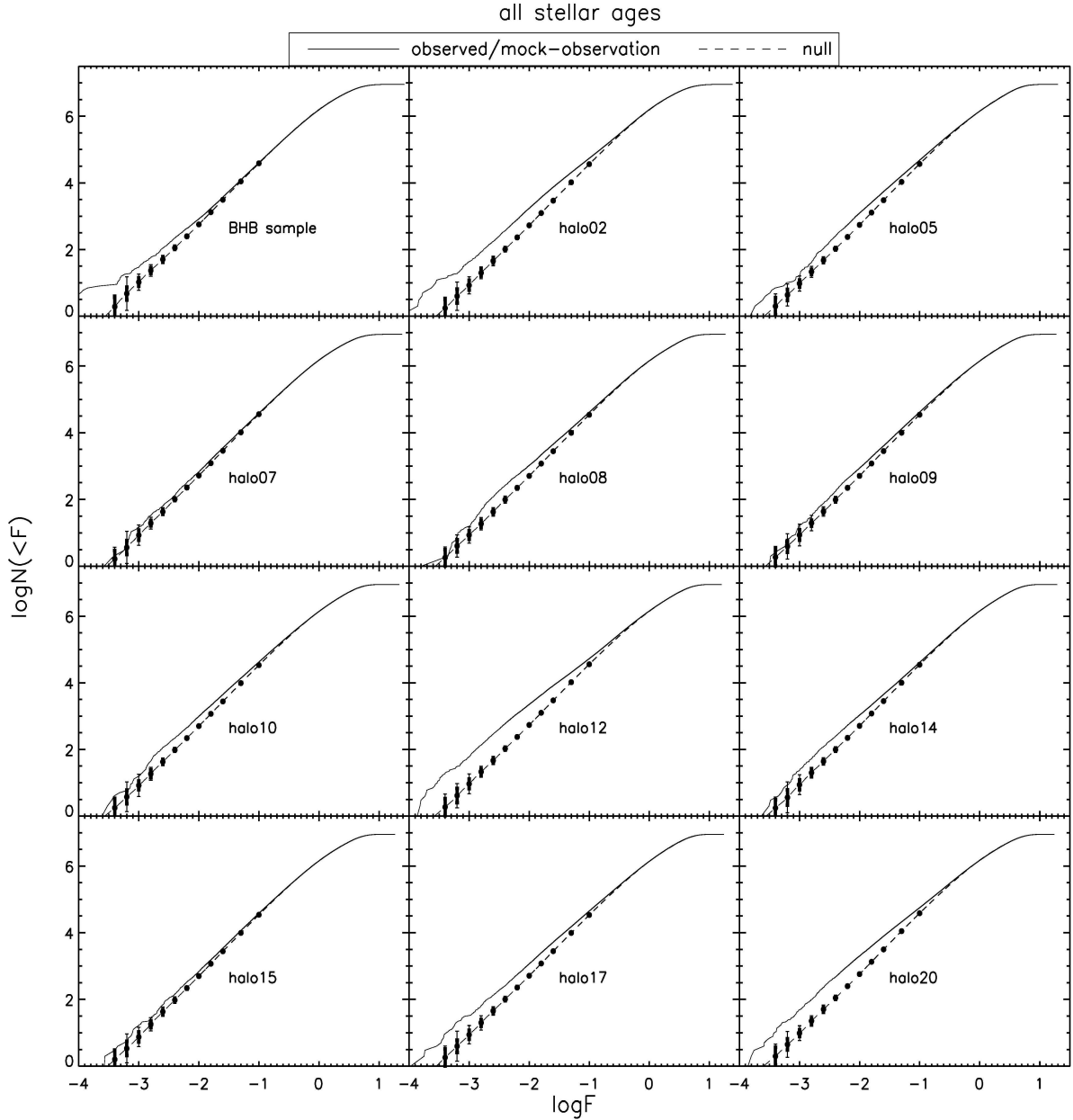


Fig. 6.— Data-model comparison for the position-velocity substructure. In each panel (one with real data and 11 with mock-data from BJ05), we show the cumulative distribution of the four-distance F (Eq. 1), as in Figure 4. The simulations were sampled in angular coverage and distance distribution to resemble the actual BHB sample. Solid lines are the cumulative distribution of F for the observations or mock-observations, while the dashed lines are the average cumulative distributions of F for 100 null hypotheses, as in the previous figures. This figure shows that there is considerable variation in $N(< F)$ *vs.* $N(< F_0)$ among the different realizations simulated by BJ05, but that all simulations exhibit position-velocity clustering as an excess of $N(< F)$ for small F . The observed position-velocity substructure (top left panel) resembles that seen in the simulations, where the halo is exclusively made up from disrupted satellites.

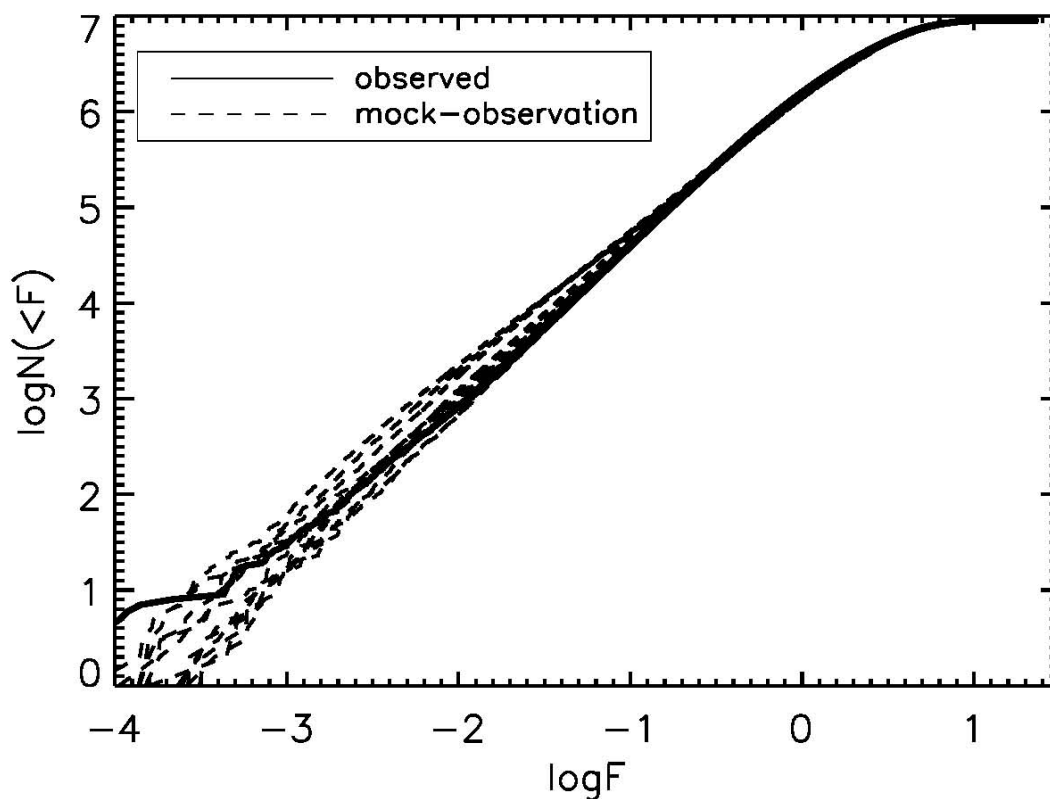


Fig. 7.— Close pair distribution for the observed BHB sample and the 11 simulations. The solid line is the cumulative distribution of F for the actually observed BHB sample; the dashed lines are the F distributions for the mock-observations of the 11 simulations. Overall, the observations fall well within the range of expectation from the BJ05 simulations, but the simulations have somewhat more mid-scale power ($\log F \sim -2$ to -1) than the observations.

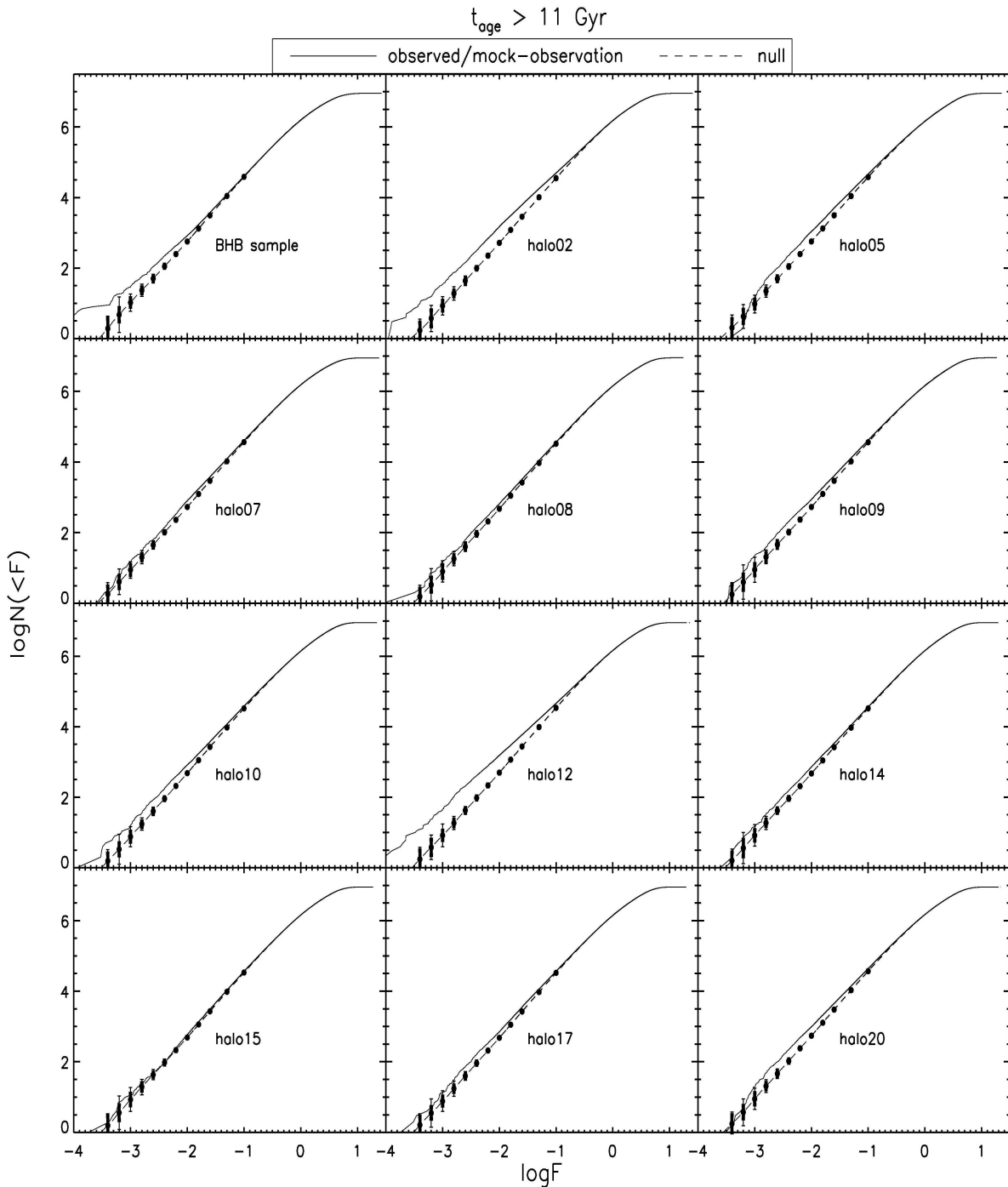


Fig. 8.— Close pair distributions for the BHB sample and particles older than 11 Gyr in each of the 11 BJ05 simulations. The solid lines are the cumulative distributions of F for the observation or mock-observations, while dashed lines are corresponding average cumulative distributions of F for 100 null hypotheses. Clearly, the observation is consistent with the older parts of most simulations (except for halo02 and halo12).

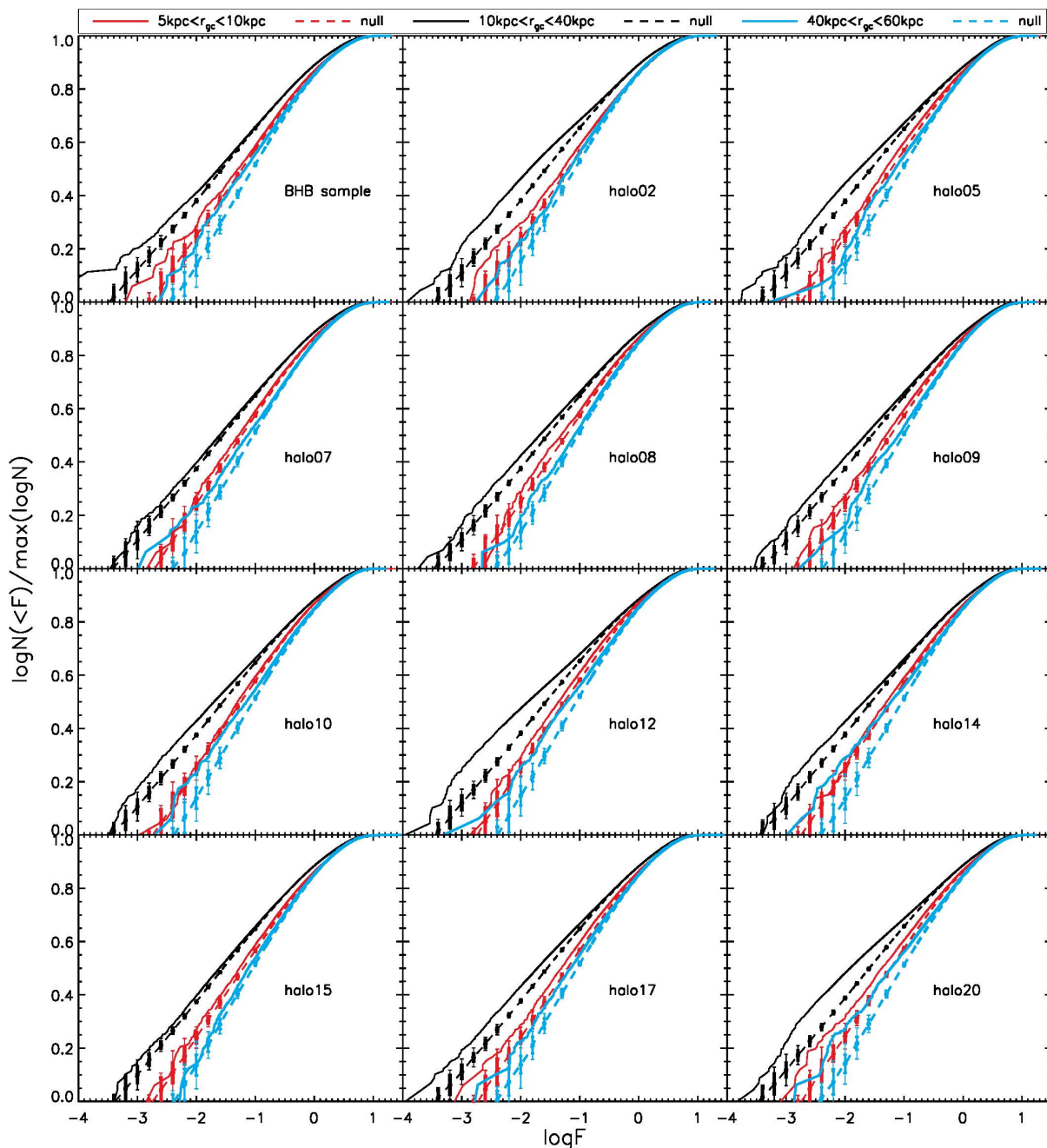


Fig. 9.— Close pair distribution of F for BHB stars and the 11 BJ05 simulations in regions that should be dominated by the outer-halo (subsample II: $10 \text{ kpc} < r_{\text{gc}} < 40 \text{ kpc}$; black lines and subsample III: $40 \text{ kpc} < r_{\text{gc}} < 60 \text{ kpc}$; blue lines) and inner-halo (subsample I: $5 \text{ kpc} < r_{\text{gc}} < 10 \text{ kpc}$; red lines) populations, respectively. The dashed lines are the corresponding average cumulative distributions of F for 100 null hypotheses. The filled circles locate the mean of the 100 null hypotheses; the thick error bars enclose 68% of the distribution, while the thin error bars enclose 95% of the null hypotheses. The figure shows that the outer halo exhibits a more pronounced substructure signal than the inner halo for all simulations. However, the actual level of $N(< F)$ depends on the projected sky density of particles as a function of their distance, because we mocked the same density as BHB stars.